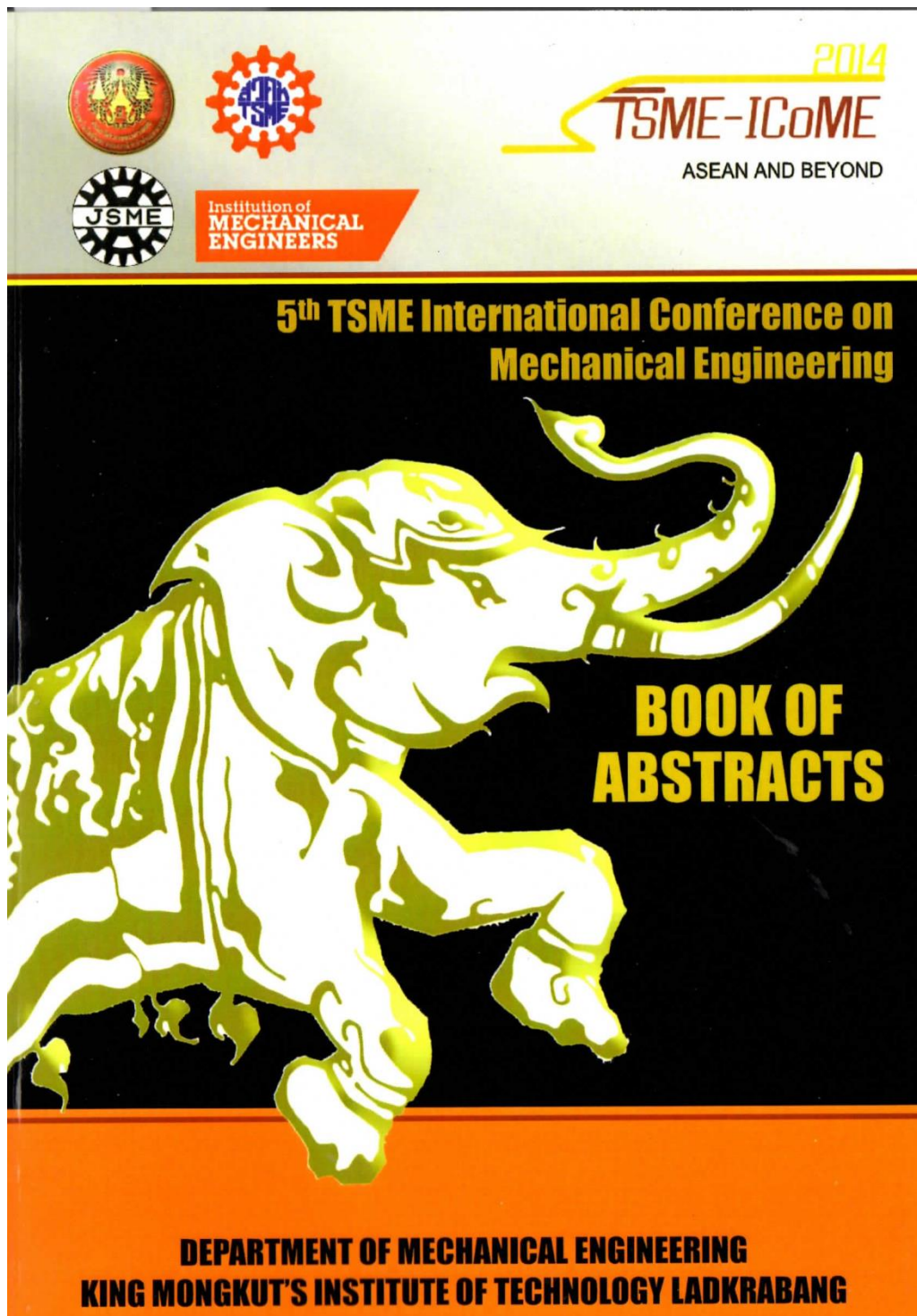


ภาคผนวก ก

การตีพิมพ์ที่ได้รับการเผยแพร่



Abstract Content (Continue)

The 5th TSME International Conference on Mechanical Engineering

	Page
AMM057	68
3-D Structural Analysis of an Electric Three-wheeled Vehicle Integrating with a Battery Switching System Narin Chaitanas, Anon Phunglila, Phayaporn Leelapichaihan, Ek-ut Thammakornburiel, Sombor Tanaka, Nutapol Lingsriyansak	
AMM058	69
New Applications of Woodceramics Originated from Waste Thai Hevea Wood Doo Kwanbock, Masahito Otake, Toshihiro Otake, Akiko Takasaki	
AMM059	70
Estimation of Carbon Fiber Surface Energy using Standard Probe-Liquid Technique Ponbtep Pattanasawatitjgul, Kot Jantiprach	
Biomechanics: BME	
BME001	72
A Review of Computer Simulation of Spine Biomechanics for the Treatment of Scoliosis Athawa Jakkun, Ian Gibson, Eng Heok Foy, Gabriel Liza	
BME003	73
Effectiveness of Milled-insole in Plantar Pressure Reduction Pongpon Wittanasriyong, Wisut Taneechai, Monsak Pimsam, Jitamasae Poonnar	
BME005	74
Rubber Investigations for a Gastroscopy Training Kit Decho Surongprateer, Aimsan Tongpradadee, Anchasa Piamsuwanroonki	
Computation and Simulation Techniques: CST	
CST001	76
Heat Conduction Analysis in Three-Dimensional Solid by Control Volume Finite Element Method Passakorn Vessakosol	
CST004	77
Modeling of Double-ellipsoidal Heat Source for Submerged Arc Welding Process Nareedon Kitapornvittitreegron, Chaitrong Sukumwong	
CST005	78
Numerical Simulation of Heat Transfer Process in Oil-immersed Transformer Pavlan Tangyoo, Chaitrong Sukumwong	
CST006	79
Numerical Analysis for Dynamic Characteristics of Sphere Drop Test on Oil-based Clay Backing Material Chasen Chakrimgong, Chaitrong Sukumwong	
CST007	80
Numerical Investigation on Heat and Water Transport in PEM Fuel Cell Keeasat Sattanasak, Jitmasae Chaitongrak	
CST008	81
Effect of Wheel Attack Angle on Flange Climb Derailment Criteria using Finite Element Method Monsak Pimsam, Sornthai Gongrak	
CST010	82
Verification and CFD Modeling of Airflow and Temperature Distribution in Enclosed Space Krenet Sittasart, Krenet Sukkasa, Preecha Wiamong, Pongwat Wichamaung	

Abstract Content (Continue)

The 5th TSME International Conference on Mechanical Engineering

	Page
CST011	83
A Molecular Dynamics Study of Proton Hopping in Polymer Electrolyte Membranes Taksay Meibach, Takashi Takemasa	
CST014	84
Simulation and Experiment on Effective Excitation of Mobile Phone Panels Yoshihiko Kaku, Shinya Honda, Yoshitomo Naito	
CST015	85
Optimization of Partion Thickness for Extrusion Blow Molding of a Rectangular Shape Bottle Using FEM and AI Technique Ravitat Rigai, Chait Suvanyumrat	
CST020	86
Study of Rail Vehicle Dynamic Response: A Computational Approach Bikron Hazarka, Monsak Pimsam	
CST021	87
Dimension Ratio of Including Jet for Gas-liquid Mixing Kewat Krasumitamon, Nutvapa Jitvanakachai, Chinsut Thanpong	
CST022	88
A Study on Passenger Bus Superstructure Strength for Rollover Test Suchanot Kongwat, Bowornan Chawanwan, Kewat Vajayonata, Pattaramon Jongsomrat	
CST023	89
Methane Jet Flame Simulation Using C++ Open Source Codes of Computational Fluid Dynamics Software Pant Kemma, Chait Suvanyumrat	
CST024	90
Wave Forces on Large Cylindrical Structure Using CFD Simulation Charata Nonsat, Sornchai Chocheepsakul, Duangpordee Kiatgajjalong	
CST025	91
Exact Stiffness Matrix for Modified Strain-gradient Bars Embedded in Elastic Substrate Media: The Virtual Force Derivation Suchart Limabanyu	
CST026	92
Description of User-defined Material Subroutine (UMAT) in LS-DYNA for Nonlinear Solid Mechanics Anucha Promsuegphra, Palboon Umpitjanich	
Dynamic systems, Robotics and Control: DRC	
DRC001	94
Robust Speed Control of a Single-cylinder Gasoline Engine Pant Ngamson, Akasong Jitpong	
DRC002	95
A Robust Control with Adaptive Controller Output Reduction Pant Ngamson	
DRC003	96
Quantitative Feedback Control of a Diesel Engine Throttle Witit Chaitanaguchai, Surawit Meenukongyong	

CST021

The 5th TSME International Conference on Mechanical Engineering
17-19th December 2014, The Empress, Chiang Mai



Dimension Ratio of Inducing Jet for Gas-liquid Mixing

Keerati Kirasamutranon^{1,*}, Nuthvipa Jayranaiwachira¹ and Chinaruk Thianpong¹

Department of Mechanical Engineering, Faculty of Engineering,
King Mongkut's Institute of Technology Ladkrabang, Bangkok 10520, Thailand

*Corresponding Author: pringles_note@hotmail.com

Abstract

By injecting high velocity water as the primary fluid through the vertical down-flow ejector, the pressure around the ejector is dropped and entrained the surrounding air to mix with the liquid. In this work, effects of dimension ratios of liquid jet ejector to the air suction rate were investigated. The Computational Fluid Dynamics (CFD) models have been used to obtain the results and validated with experiments. Dimensions of ejector are studied in terms of nozzle diameter (D_j), diameter (D_c) and length (L_c) of mixing chamber, air inlet diameter (D_a) and position of air inlet referred to nozzle edge (L_a). Both simulation and experimental results show that dimension ratios which give the highest air suction rate with every water flow rates are $D_c=3D_j$, $L_c=6D_j$, $L_a=2D_j$ and $D_a=2.5D_j$. According to these dimension ratios, the performance of the ejector in air inducing are 0.36, 0.31, 0.25 and 0.19 kg air/kW-h at water flow rates of 20.10, 18.67, 17.24 and 15.81 L/min, respectively.

Keywords: Ejector, Air suction volume, Pressure

CST021

The 5th TSME International Conference on Mechanical Engineering
17-19th December 2014, The Empress, Chiang Mai



DIMENSION RATIO OF INDUCING JET FOR GAS-LIQUID MIXING

Keerati Kirasamutranon, Nuthvipa Jayranaiwachira and Chinaruk Thianpong*

Department of Mechanical Engineering, Faculty of Engineering,
King Mongkut's Institute of Technology Ladkrabang, Bangkok 10520, Thailand

Abstract

By injecting high velocity water as the primary fluid through the vertical down-flow ejector, the pressure around the ejector is dropped and entrained the surrounding air to mix with the liquid. In this work, effects of dimension ratios of liquid jet ejector to the air suction rate were investigated. The Computational Fluid Dynamics (CFD) models have been used to obtain the results and validated with experiments. Dimensions of ejector are studied in terms of nozzle diameter (D_n), diameter (D_c) and length (L_c) of mixing chamber, air inlet diameter (D_a) and position of air inlet referred to nozzle edge (L_a). Both simulation and experimental results show that dimension ratios which give the highest air suction rate with every water flow rates are $D_c=3D_n$, $L_c=6D_n$, $L_a=2D_n$ and $D_a=2.5D_n$. According to these dimension ratios, the performance of the ejector in air inducing are 0.36, 0.31, 0.25 and 0.19 kg air/kW-h at water flow rates of 20.10, 18.67, 17.24 and 15.81 L/min, respectively.

Keywords: Ejector, Air suction volume, Pressure

1. Introduction

An ejector is a device in which a high-pressure fluid jet is used to entrain low-pressure fluid. Fig. 1 shows a schematic drawing of typical ejector [1]. Which consists of four main components: one inlet for high-pressure water; another inlet for air/abrasive; a mixing chamber and a mixing tube. Due to their simple design and the absence of moving parts, ejectors are very reliable device having practically no maintenance cost and relatively low installation cost [2]. According to the Bernoulli's principle, when a motive fluid is pumped through the nozzle of a gas-liquid ejector at a high velocity, a low pressure region is created just outside the nozzle. A second fluid gets entrained into the ejector through this low pressure region. Ejectors are

being used as a gas-liquid dispersion device for many purposes for a very long time in the chemical industries since it has high mass transfer and mixing rates.

Many CFD works have been carried out to determine the performance of ejectors [3, 4, 5, 6] but they are mainly focused on mono-phase (gas-gas or liquid-liquid) ejector except the study of Kandakure et al [7]. Some of them assumed the two-phase flow (water jet and air) is a homogeneous fluid, and hence non experimentations were conducted [8, 9]. Moreover, in the literature, there are a few experimental studies dealing with the behaviour of low-pressure water jet in the tube. For instance, Miller et al [10].

CST021

Therefore, in the present study, effects of dimension ratios of liquid jet ejector to the air suction rate were investigated. The Computational Fluid Dynamics (CFD) enables the prediction of local pressures in the ejectors and experiments the performance of the ejector in air induce

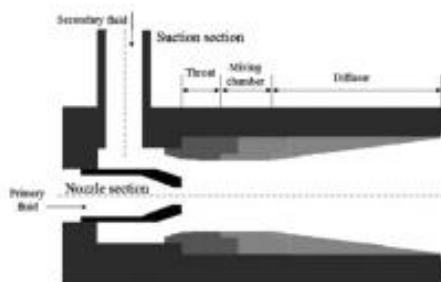


Fig. 1 Schematic diagram of a typical ejector.[1]

2. Modeling approach and boundary condition

The commercial package, Gambit 2.4.6 and Fluent 6.3., are used as the grid generator and the CFD solver, respectively. Two-dimensional geometry was considered with the quadrilateral-meshing scheme.

The mesh and model were created in a two-dimension domain. The geometries of the computational domain of the modeled liquid ejectors were taken from those which were used in the experiment. The mesh was made of about 60,000-80,000 structured quadrilateral elements and adapted by the solution-adaptive mesh refinement as shown in Fig. 2

The continuous phase from the nozzle section is water. Since the volumetric flow rates of water through the nozzle are known, the inlet velocity was used as a boundary condition. The ejector outlet was considered at the outlet pressure. The no-slip boundary condition was

enforced at the walls of the ejector. The solution was iterated until convergence was achieved, such that the residual for each equation fell below 10^{-5} .

A comprehensive model settings summary is reported in Table 1.

Table 1

Summary of the applied numerical settings.

Model settings	
Time dependence	Steady State
Viscous model	Turbulent
Turbulence model	Standard k-ε model
Numerical Settings	
Pressure	2nd order
Momentum	2nd order
Turbulent kinetic energy	2nd order
Turbulent dissipation rate	2nd order

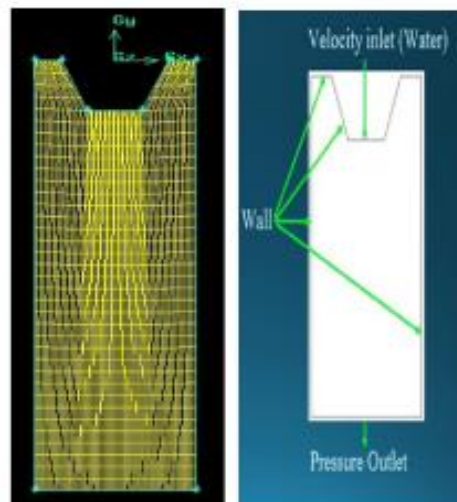


Fig. 2 Grid structures and boundary condition of the ejector CFD model.

CST021

3. Experimental setup

The validation experiment is carried with an acrylic column of 0.40 m in diameter and 0.9 m in height (Fig 3(A)). The ejector made of Aluminum as shown in Fig. 3(B). The water flow rate was manually controlled with the help of a calibrated Rota meter show in Fig. 3(C) (Nitto Instruments Model Z-500 make with accuracy of 5%). The velocity of air flowing through the nozzle was varied over a wide range. The air flow rate was manually measure with the Thermo anemometer is shown in Fig. 3(D) Table 2 shows the various geometry parameters that were investigated.

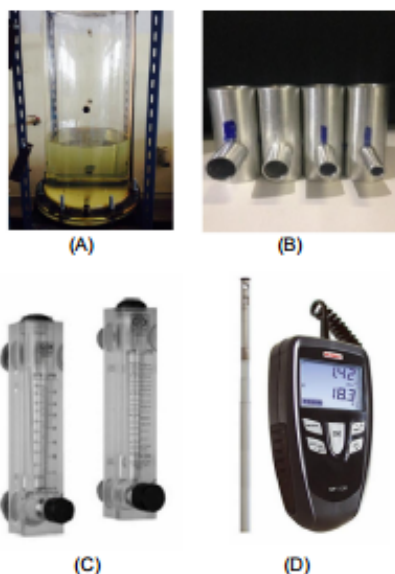


Fig. 3. (A) Acrylic column, (B) Ejector,
(C) Rota meter, (D) Anemometer

Table 2

Dimensions of the ejector and parameters varied in the CFD and experiments

Parameter	Values
Nozzle inlet diameter D (mm)	12
Nozzle diameter D_j (mm)	6
Mixing chamber diameter D_c (mm)	$3D_j$, $4D_j$, $5D_j$
Mixing chamber length L_c (mm)	$3D_j$, $6D_j$, $9D_j$
Air inlet diameter D_a (mm)	$1D_j$, $1.5D_j$, $2D_j$, $2.5D_j$
Position of air inlet referred to nozzle edge L_a (mm)	$1D_j$, $2D_j$, $3D_j$
liquid velocity inlet (L/min)	15.81, 17.24, 18.67, 20.10

4. Results and discussion

4.1 Numerical simulation results

The CFD, therefore, enables the prediction of local pressures in the ejectors, which are otherwise very difficult to measure.

Thus, for example, the ratio of nozzle (D_j) to mixing chamber is one of the important parameters for the ejector design. Interior flow regimes in the liquid ejector can be obtained from the CFD simulation. The performance of CFD simulation, the ratio of nozzle to mixing chamber $D_c=3D_j$, $L_c=6D_j$ is the best ratio. Due to the size integrity of the core jet and the distribution of the jet without into walls. The CFD results show that the expedient model is as shown in Fig 4(A) the contour of mixture velocity magnitude in high liquid velocity jet and Fig. 4(B) the contour of static pressure in the ejectors, for constant liquid flow rate of 20.10 L/min.

Comparison of CFD predicted pressure drop and velocity jet results for constant liquid flow rate of 20.10, 18.67, 17.24, 15.81 L/min., for the ratio of nozzle to mixing chamber $D_c=3D_j$, $L_c=6D_j$.

CST021

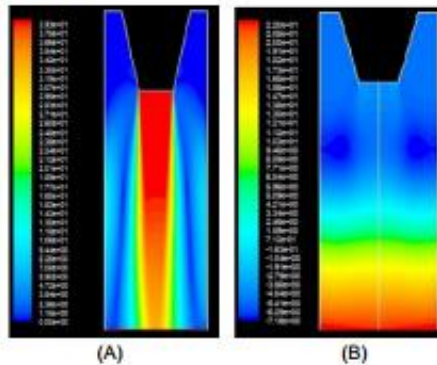


Fig. 4 CFD predicted (A) velocity magnitude (B) static pressure for $D_2=3D_1$, $L_2=6D_1$, 20.10 L/min.

The results show that the ratio of the nozzle diameter to the Mixing chamber diameter plays a crucial role in determining the hydro-dynamics and the performance of the ejectors.

As shown in Figs.5–6 shows the comparison of the predicted values of the ratio of nozzle to mixing chamber $D_2=3D_1$, $L_2=6D_1$. Fig. 5 shows Comparisons of Pressure and Lengths of the wall. When a motive fluid through the nozzle at a velocity, a low pressure region is created just outside the nozzle, the distance from the wall 0.02 m. When the water flow rate is increase, the pressure in the ejector also a decrease.

As can be seen from the Fig. 6 shows the performance of the predicted values of velocity cores of jet and position of referred to nozzle edge. Moreover, a low pressure region is created just outside the nozzle, a velocity behind position 0.02 m. from center the ejector velocity drop.

Therefore, the CFD results (Figs.4–6) shows proper placement of the air hole points of low pressure in the ejector around the wall is - 0.02 m., which is 12 mm. from nozzle all cases. So the appropriate ratio air hole is $2D_1$.

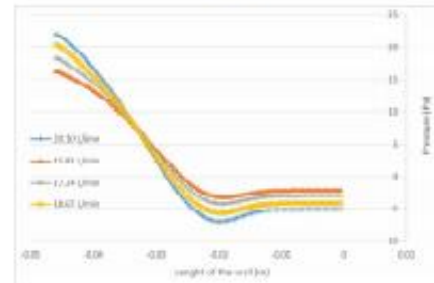


Fig. 5 Comparison of CFD predicted Pressure and lengths of the wall, The ratio of nozzle to mixing chamber $D_2=3D_1$, $L_2=6D_1$ at liquid flow rates of 20.10, 18.67, 17.24 and 15.81 L/min, respectively.

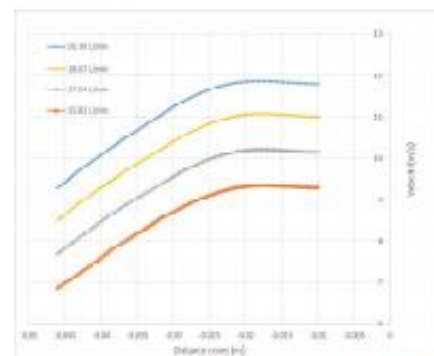


Fig. 6 Comparison of CFD predicted velocity cores of jet and position of referred to nozzle edge, The ratio of nozzle to mixing chamber $D_2=3D_1$, $L_2=6D_1$ at liquid flow rates of 20.10, 18.67, 17.24 and 15.81 L/min, respectively.

The pressure around the ejector is dropped and entrained the surrounding air, flow rate can be calculated from Bernoulli equation by considering the lowest pressure. Consequently, the pressure that use in calculation is the lowest pressure of the first point (Fig.5) and second point is atmospheric pressure. Air inlet diameter (D_1) is $2D_1$.

CST021

From Bernoulli's Equation. (1)

$$\frac{P_1}{\rho_a g} + \frac{v_1^2}{2g} + z_1 = \frac{P_2}{\rho_a g} + \frac{v_2^2}{2g} + z_2$$

$$\frac{v_1^2}{2g} = \frac{P_2 - P_1}{\rho_a g} + \frac{v_2^2}{2g} + (z_2 - z_1)$$

$$v_1^2 - 2g \left(\frac{P_2 - P_1}{\rho_a g} + \frac{v_2^2}{2g} + (z_2 - z_1) \right) \quad (1)$$

$$Q = Av \quad (2)$$

Second equation set in First equation

$$\left(\frac{Q_1}{A_1} \right)^2 = 2g \left(\frac{P_2 - P_1}{\rho_a g} + \frac{v_2^2}{2g} + (z_2 - z_1) \right) \quad (3)$$

When the second point is atmospheric pressure and dramatically low flow rate

$$Q_{a, \text{sim}} = A_1 \sqrt{2g \left(\frac{-P_1}{\rho_a g} + (z_2 - z_1) \right)} \quad (4)$$

And $D_s = 12 \text{ mm}$, $A = 0.0000113 \text{ m}^2$ and $z_1 = z_2$

$$Q_{a, \text{sim}} = 6.78 \sqrt{\frac{-P_1}{\rho_a}} \quad (5)$$

When

$Q_{a, \text{sim}}$ = Flow rate of air from calculation (l/min),
 P_1 = the lowest pressure from the graph of flow rate (N/m^2), P_a = Density of air = $1.18 \text{ (kg/m}^3)$

Flow rate of air which obtains from calculation is shown in table 3 and flow rate of air is calculated from the lowest pressure of each flow rate. Therefore, when the position of hole air is changed (L_s) becomes $1D_s$, $2D_s$ and $3D_s$ therefore, it can show relationship with flow rate of water in Fig. 7 However, this relationship can be changed to depend on independent variables by Reynolds number for easier consideration. In addition, this method can be used in many conditions that is shown in Fig. 8.

According to Fig. 7 and 8 show the positions of holes air (L_s) that make flow rate of air is the highest at $2D_s$, $1D_s$ and $3D_s$ respectively. Moreover, the graph seems to be linear because the ability of both fluids has an effect on the ability of induction that is shown in Reynolds number's graph.

Table 3

Flow rate of air from calculation

Liquid flow rate (L/min)	Air flow rate (L/min)		
	$L_s=1D_s$	$L_s=2D_s$	$L_s=3D_s$
20.1	21.6	23.2	20.1
18.67	20.1	21.6	18.5
17.24	18.5	20.1	16.9
15.81	16.9	18.7	15.5

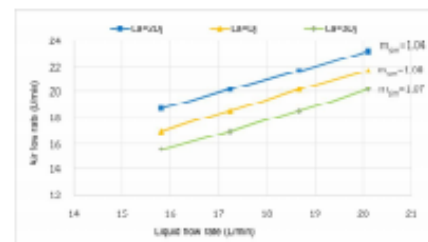


Fig. 7 The relationship between flow rate of water and air from calculation

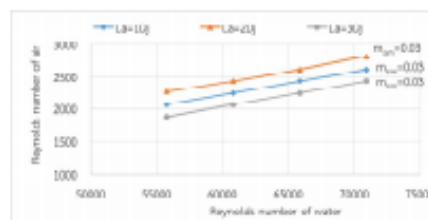


Fig. 8 The relationship between Reynolds numbers of water and air in L_s from calculation

4.2 Experimental results

The experiment tests with the 6 mm injection and mixing chamber diameter 18 mm. ($D_c = 3D_s$) mixing chamber length 36 mm. ($L_c = 6D_s$) diameter

CST021

of hole air is 12 mm. and the position of hole air is $1D_j$, $2D_j$ and $3D_j$ for finding properly position of hole air when flow rate of water is 20.1, 18.67, 17.24 and 15.81 L/min. The result of experiment is shown in Fig. 9. Consequently, it shows relationship between flow rate of water and air in L/min.

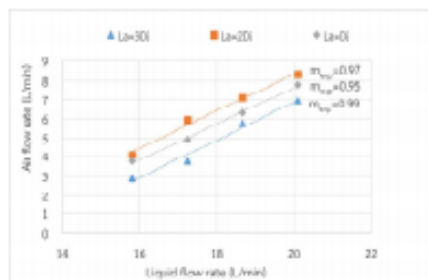


Fig. 9 Relationship between air flow rate and water flow rate at different L_a from experiment

It can be seen from the Fig. 9 that show the position of holes air (L_a) is $2D_j$ and air flow rate which is induced is the highest flow rate. Therefore, it relates with the result of the model in Fig.7 and flow rate also drops at the position of holes air $1D_j$ and $3D_j$ respectively.

The ratio of air flow rate and water flow rate which obtains from experiment at different air inlets is compared the result with the result of the model in Fig. 10. Moreover, Reynolds number of air and water that get from experiment at different air inlets is also compared with the model in Fig. 11. The best way to find diameter of holes air (D_a) from experiment is specifying size of diameter injection (D_j) at 6mm., in addition, diameter and mixing chamber length (D_c and L_c) are 18 mm. ($3D_j$) and 36 mm. ($6D_j$) respectively.

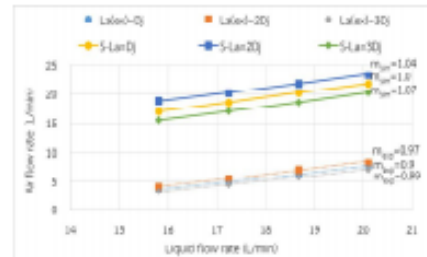


Fig. 10 The comparison between the experiment and the model of different holes air position in air flow rate and water flow rate

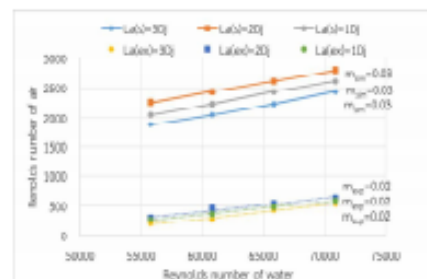


Fig. 11 The comparison between the experiment and the model of different holes air position in Reynolds number of air and water.

Lastly the position of holes air is 12 mm. ($2D_j$) from the end of injection (Fig. 10). The flow rates are 20.10, 18.67, 17.24 and 15.81 L/min. Moreover, this experiment tests a change of diameter size of holes air (D_a) in 4 times ($1D_j$, $1.5D_j$, $2D_j$ and $2.5D_j$) that is shown in Fig. 12

The relationship between flow rate of air and water from experiment that is tested by different diameters of holes air (D_a) $1D_j$, $1.5D_j$, $2D_j$ and $2.5D_j$ show in relation with independent variables and Reynolds number in Fig. 13.

CST021

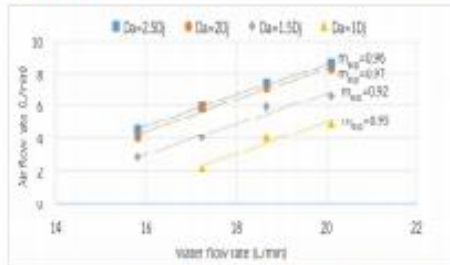


Fig. 12 The relationship between flow rate of water and air at different densities (D_a)

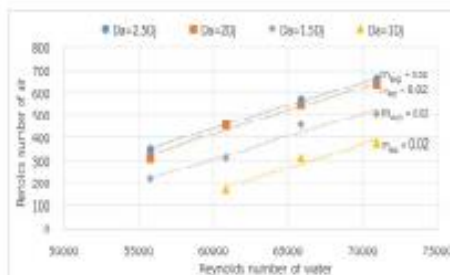


Fig. 13 The relationship between Reynolds number of water and air at different densities (D_a)

Capability of filling in air shows in unit of kilogram O_2 per kilowatt hour and it is tested by calculating quantity of power that spends on system and it is measured by clamp on power meter. As a result, the result of filling air is shown in the table 4 and the maximum capability of filling is $0.36 \text{ kg } O_2 / \text{kWh}$. The system of filling air which uses in industry has ability number of filling air about $0.6\text{-}3.9 \text{ kg } O_2 / \text{kWh}$.

Taking a picture of air bubble for considering size of air bubble is essential because size of air bubble has influence on ventilating of water. Therefore, studying size of air bubble will be studied by taking a picture with a camera

(Canon EOS 7D) and water flow rate is 20.1, 18.67, 17.24 and 15.81 L/min.

For example, size of air bubble at L_a is $2D_j$ and water flow rate (Q_w) is 20.1, 18.67, 17.24 and 15.81 L/min. in figure 14 (A), (B), (C) and (D) respectively.

Table 4

Water flow rate compares with performance of the ejector in air

Water flow rate (L/min)	Performance of the ejector in air ($\text{kg } O_2 / \text{kWh}$)
20.1	0.36
18.67	0.31
17.24	0.25
15.81	0.19

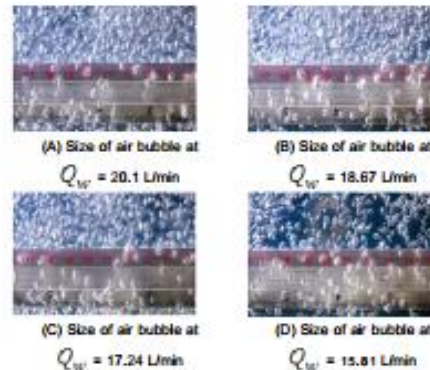


Fig. 14 (A), (B), (C) and (D) Size of air bubble at $L_a = 2D_j$

Size of air bubble from taking a picture by a camera (Canon EOS 7D) obtain a lot of size of air bubble from different flow rate, air bubble and position of hole air. Therefore, size of air bubble has similar size about 2-3 mm.

CST021

5. Conclusions

In the present work, water flow rate at 20.1, 18.7, 17.2 and 15.8 L/min give the best mass flow rate \dot{O}_2 /input of power electric at 0.36, 0.31, 0.25 and 0.19 $\text{kg } \dot{O}_2 / \text{k}_{\text{watt}} \text{ hr}$ respectively. Moreover, the best of performance of the ejector in air is water flow rate at 20.1 L/min. and the best dimension ratio of performance of the ejector in air is $D_c=3D_j$, $L_c=6D_j$, $L_a=2D_j$ and $D_a=2.5D_j$.

Moreover, in the model that creates at water flow rate 20.10, 18.67, 17.24 and 15.81 L/min give the best mass flow rate \dot{O}_2 /input of power electric at water flow rate 20.10 L/min as an experiment of the dimension ratio that is also the same way.

The ability of main fluid that uses performance of the ejector with unimportant fluid affects to flow rate. Consequently, it can be determined from graph of Reynolds number which can change flow rate to be independent variables by adding variables (density of fluid and viscosity). From the graph, if the main fluid has high density and a lot lower viscosity than unimportant fluid, it will cause Reynolds number of unimportant fluid to increase. As a result, it will increase flow rate too.

From the picture of air bubble, it shows similar size of air bubble in many sizes of injection and a lot of flow rate. Moreover, the size of air bubble is about 2-3 mm. as a result, it is small air bubble that works very well with the system of filling air.

6. References

- [1] Havelka, P., Linek, K., Sinkle, J., Zahradnik, J., Fialova, M. (1997). Effect of the ejector configuration on the gas suction rate and gas hold-up in ejector loop reactors, *Chemical Engineering Science*, vol.52(11), June 1997, pp. 1701–1713.
- [2] Aly, N.H., Karameldin, A., Shamloul, M.M. (1999). Modeling and simulation of steam jet ejectors, *Desalination* vol.123(1), August 1999, pp.1–8.
- [3] Riffat, S.B., Omer, S.A. (2001). CFD modeling and experimental investigation of an ejector refrigeration system using methanol as the working fluid, *International Journal of Energy Research* vol.25(2), February 2001, pp.115–128.
- [4] Ouzzane, M., Aidoun, Z. (2003). Model development and numerical procedure for detailed ejector analysis and design. *Applied Thermal Engineering* vol.23(18), December 2003 pp. 2337–2351.
- [5] Rusly, E., Aye, L., Charters, W.W.S., Ooi, A. (2005). CFD analysis of ejector in combined ejector cooling system, *International Journal of Refrigeration*, vol.28(7), November 2005, pp.1092–1101.
- [6] Sriveerakul, T., Aphornratana, S., Chunnanond, K. (2007). Performance prediction of steam ejector using computational fluid dynamics: part 1. Validation of the CFD results, *International Journal of Thermal Science* vol.46(8), August 2007, pp.812–822.
- [7] Kandakure, M.T., Galkar, V.G., Patwardhan, A.W. (2005). Hydrodynamic aspects of ejectors, *Chemical Engineering Science*, vol.60(22), November 2005, pp.6391–6402.

CST021

[8] Tazibt, A., Abriak, N, Parsy, F. (1996). Prediction of abrasive particle velocity in a high pressure water jet and effect of air on acceleration process, *European Journal of Mechanics - B/Fluids*, vol.15(4) pp. 527–543.

[9] Raissi, K. (1989). Mixing tube geometry influence on abrasive water jetflow, in: C. Gee (Ed.), *Proc., 13th Int. Jet Cutting Tech-nol.*, BHRA Fluid Engineering, October 29–31, Italy.

[10] Miller, A L. (1989) The dynamics of multi-phaseflow in collimated jets, in: M.M. Vijay (Ed.), *Proc. 5th American Water Jet Conf.*, August 29–31, Canada.